

# PromptHSI: Universal Hyperspectral Image Restoration Framework for Composite Degradation

Chia-Ming Lee<sup>1</sup>, Ching-Heng Cheng<sup>1</sup>, Yu-Fan Lin<sup>1</sup>, Yi-Ching Cheng<sup>1</sup>, Wo-Ting Liao<sup>1</sup>,  
Chih-Chung Hsu<sup>†1</sup>, Fu-En Yang<sup>2,3</sup>, Yu-Chiang Frank Wang<sup>2,3</sup>

Institute of Data Science, National Cheng Kung University<sup>1</sup>

Graduate Institute of Communication Engineering, National Taiwan University<sup>2</sup> NVIDIA<sup>3</sup>

## Abstract

Recent developments in All-in-One (AiO) RGB image restoration and prompt learning have enabled the representation of distinct degradations through prompts, allowing degraded images to be effectively addressed by a single restoration model. However, this paradigm faces significant challenges when transferring to hyperspectral image (HSI) restoration tasks due to: 1) the domain gap between RGB and HSI features and difference on their structures, 2) information loss in visual prompts under severe composite degradations, and 3) difficulties in capturing HSI-specific degradation representations through text prompts. To address these challenges, we propose **PromptHSI**, the first universal AiO HSI restoration framework. By leveraging the frequency-aware feature modulation based on characteristics of HSI degradations, we decompose text prompts into intensity and bias controllers to effectively guide the restoration process while avoiding domain gaps. Our unified architecture excels at both fine-grained recovery and global information restoration tasks. Experimental results demonstrate superior performance under various degradation combinations, indicating great potential for practical remote sensing applications. The source code will be publicly released.

## 1. Introduction

Hyperspectral images encompass a greater number of spectral bands than RGB images, offering extensive spectral details [44]. Because materials reflect different spectral bands, each substance can have a unique signature for material identification [1, 32, 37, 44]. HSI can capture these valuable information and has broad application value and potential. However, because of the limitation of the device

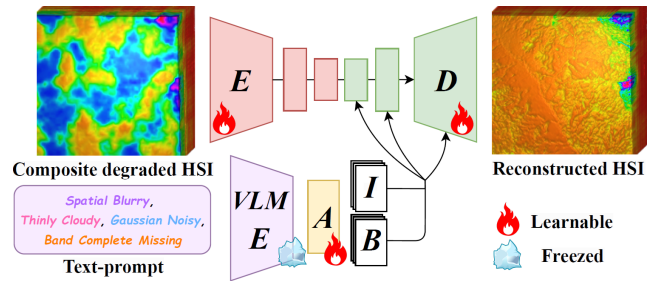


Figure 1. The All-in-One and universal HSI restoration framework with text-prompt guidance, named PromptHSI, for composite degradation. Specifically, informative textual features extracted by pre-trained vision-language model are fed into adapter and then decomposed into an intensity and bias embeddings for degradation-specific restoration with effective cascade guidance.

and bandwidth, observed HSIs are usually damaged by different types of degradation from camera sensing and transmission. Thus, HSI restoration is a crucial pre-processing step to recover degraded pixels from flawed observations.

Previous works tended to be based on HSI structures, low-rank sparsity prior [11, 42, 43] for specific degradations such as Gaussian noise [25, 49], stripe effect [22, 24], spatial blurring [19, 33], and cloud occlusion [35, 48]. However, in real-world scenario, HSIs are easily prone to multiple types of degradation, causing these methods to be limited. When HSIs are subject to multiple degradation, some methods based on deep unfolding network [4, 34] or optimization [28, 29, 42, 52] perform significantly below expectations and lack flexibility to use for real-world application.

With the development of AiO RGB image restoration methods [5, 10, 13, 31, 39], which can address multiple degradations in a single network, there is a potential to resolve this situation. However, due to the significant domain gap between the HSI and RGB images, these AiO methods cannot be transferred to HSI restoration. In particular, the visual-prompt approaches [5, 39] are influenced by severe and diverse corruptions. Furthermore, while text-prompts

<sup>†</sup>Corresponding author, email: cchsu@gs.ncku.edu.tw

[10, 13] have emerged as an effective approach for controlling All-in-One restoration models, the textual feature representations encoded by widely-used vision-language models (VLMs) pre-trained on RGB-text datasets, such as CLIP [40], exhibit significant domain gaps with HSI features. Given these limitations, leveraging prompt learning frameworks for HSI processing remains an open challenge.

Considered as a whole, the essential questions are *Can we leverage prompt learning and vision-language model (VLM) frameworks to address critical challenges in hyperspectral image processing for practical applications, such as achieving composite degradation restoration or controllable restoration through a single unified model?* The response is affirmative.

To meet these challenges, we propose PromptHSI, a frequency-aware and prompt-guided framework tailored for HSI’s unique spectral structure and degradation types. Unlike AiO RGB image restoration methods, it ensures spectral fidelity and adaptive degradation response through novel feature modulation strategies. Our universal restoration architecture effectively handles both fine-grained recovery (e.g. spatial-spectral super-resolution) and global information restoration (e.g. decloud, inpainting) within a single model; a frequency-aware feature modulation strategy that decomposes text-prompts into intensity and bias embeddings based on frequency-domain analysis, dispelling the domain gap between VLM and HSI features. In summary, our main contributions can be listed as follows:

- We present the first universal HSI restoration framework capable of handling composite degradations. Unlike existing HSI restoration methods that suffer from performance drops in composite degradations, our approach maintains consistent high performance across various degradation combinations.
- We propose a novel text-to-feature modulation mechanism that effectively leverages frequency-domain characteristics of HSI degradations. By decomposing textual features into intensity and bias controller embeddings, our method achieves superior control over the restoration process, outperforming state-of-the-art AiO RGB image restoration methods on composite degradation.
- Extensive experiments demonstrate that our method not only excels at HSI restoration under various degradation combinations but also exhibits strong generalization to unseen degradation types through flexible text-prompt control. The framework’s effectiveness is thoroughly validated through comprehensive ablation studies and comparisons with existing approaches.

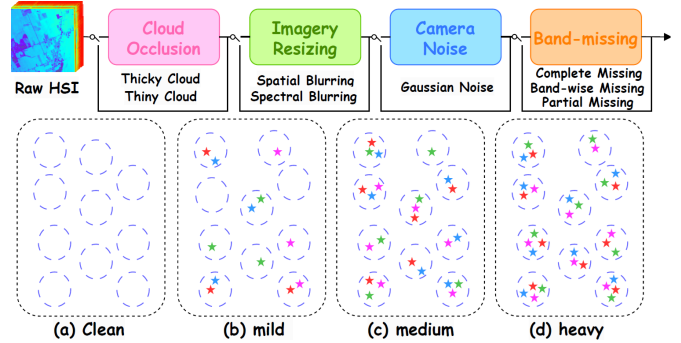


Figure 2. Illustration of the degraded HSI and corresponding description synthesis pipeline. Each degradation is activated with probability  $p$ . Note that we set  $p = 0.5$  for all experiments in this paper. To ensure diversity and realistic in the synthetic dataset, each activated degradation selects and applies one of its sub-degradations to the inputted HSI. (More detailed information and setting can be found in **Supplementary**.)

## 2. Related Works

### 2.1. Hyperspectral Image Restoration

Conventional approaches are based on the structural properties of HSI, such as low-rank and sparse priors [11, 43]. Optimization-based methods [6, 36, 42, 52] were initially used for HSI restoration. With the progress of deep learning, HSI can be effectively recovered by imposing appropriate constraints and suitable design for task-specific restoration. Unlike RGB image restoration, HSI restoration considers not only global information aggregation but also spatial-spectral correlation at locality. Several works against different types of restoration model, such as denoising [15, 24, 38] for Gaussian noise and impulse noise, inpainting [6, 29, 52] for stripe effect, and spatial blurring [18, 20, 26] or limited spectral resolution [2, 3, 14].

However, due to multiple or composite degradations that jointly affect structural information and fine-grained details of a given HSI, restoration methods are easily compromised, consistently leading to suboptimal performance.

### 2.2. All-in-One RGB Image Restoration

A recently emerging paradigm in RGB image restoration involves designing single models to restore different types of degradation [5, 7, 10, 12, 13, 23, 39]. Current techniques, as a type of multi-task learning, utilize various frameworks to manage inputs and outputs for multiple tasks with prompting methods, facilitating effective information sharing between them and corresponding degradation. Specifically, AirNet [23], the first proposed AiO image restoration method, employed contrastive learning to train the encoder to learn degradation representations and restoration with a single network. PromptIR [39] introduced the visual prompt for the degradation perception and

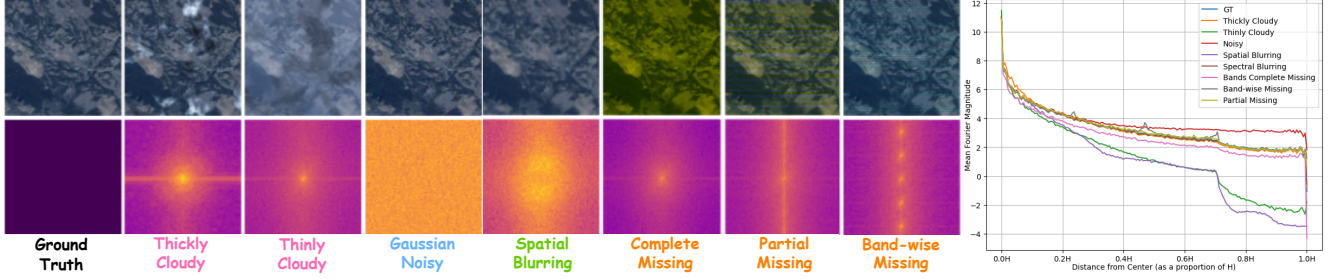


Figure 3. *Left*, displayed from top to bottom, are HSIs with specific degradation alongside the Fourier spectra of the residual images, which are derived from subtracting the degraded images from the ground truth. *Right*, the diagram presents the mean values of the Fourier spectra based on the square length indicated on the x-axis. It is evident that varying degradations focus on distinct frequency subbands.

information integration within the decoding process without a priori needs. InstructIR [10] followed the text-prompt as instruction to guide the network, archiving great results with controllability. HAIR [5] is based on the hypernetwork, which aims to generate network parameters for corresponding degradations. Recently, OneRestore [13] has extended AiO restoration from multiple degradation to composite degradation, which can address the various corruption even they exists in a same image simultaneously.

Although these methods are effective, these solutions are limited in HSIs. Due to domain gap and composite degradation, it is difficult to effectively learn the compact representation of degradation and perform effective restoration.

### 3. Preliminary and Motivation

#### 3.1. Unified HSI Restoration Network Design

For comprehensive restoration using a single network, employing an architecture suitable for various degradations is crucial [8, 47]. In RGB image restoration, two classic architectures predominate: ❶ U-shape encoder-decoder [45, 46] and ❷ plain residual-in-residual [17, 27, 50]. The former excels at capturing general representations and information, being widely used in denoising, deblurring, and inpainting, but pays less attention to fine details or repeat patterns. The latter specializes in capturing detailed spatial features at the fine-grained level, serving as the backbone for super-resolution tasks [9, 41, 51].

Previous methods have overlooked the compatibility between these two restoration models, and current AiO restoration approaches [5, 13, 39] typically focus on the former rather than integrate the joint strength of both types of network design, limiting their versatility. Besides, this limitation also extends to HSI restoration models [19, 21, 33]. Therefore, we integrate a plain residual-in-residual block into the U-net cascade decoder in the PromptHSI to maintain the advantages of both designs without compromising. The versatility of the network can be ensured accordingly.

#### 3.2. Degradations Analysis in Frequency Domain

Unlike RGB image restoration, HSI restoration requires careful consideration of spatial-spectral correlations across hundreds of bands. Our key insight comes from analyzing how different types of degradation manifest in the frequency-domain through Fourier analysis. Given a clean HSI  $I_{\text{clean}}$ , its Fourier transform can be expressed as:

$$F(I_{\text{clean}}) = F_s(I_{\text{clean}}) + iF_c(I_{\text{clean}}) \quad (1)$$

where  $F_s$  and  $F_c$  represent the sine and cosine components respectively. Through empirical analysis, as shown in Figure 3, we observed that different types of degradation exhibit distinct patterns in how they affect these frequency components.

Specifically, the relationship between degraded HSI  $I_{\text{degraded}}$  and clean HSI  $I_{\text{clean}}$  in frequency-domain can be characterized by an affine transformation:

$$F(I_{\text{degraded}}) = \hat{\lambda} \odot F(I_{\text{clean}}) + \hat{\mu} = (1 + \lambda) \odot F(I_{\text{clean}}) + \mu \quad (2)$$

where  $\odot$  denotes element-wise multiplication,  $\lambda$  and  $\mu$  are degradation-specific parameters that:  $\lambda$  represents the scaling factor that modulates frequency amplitudes,  $\mu$  is the bias term that shifts the frequency distribution.

Different types of degradation show characteristic patterns in  $\lambda$  and  $\mu$ , such as ❶ Blur mainly affects high frequencies:  $\lambda_{\text{high}} \ll \mu_{\text{low}}$ . ❷ Noise adds uniform perturbations:  $\mu_{\text{noise}} \approx \text{constant } c$ . ❸ Missing information creates structured patterns in both  $\lambda$  and  $\mu$ .

### 4. Proposed Method

**Overview.** Figure 4 illustrates the overall architecture of PromptHSI, which consists of three key components designed to address the challenges in universal HSI restoration: ❶ A unified U-shape network which contains Spatial-Spectral Aware Feature Extraction Block (SSAEFB) and Prompt-guided Feature Aggregation Block (PGFAB) that effectively captures both enhanced spatial-spectral fine-grained details and global contextual information from

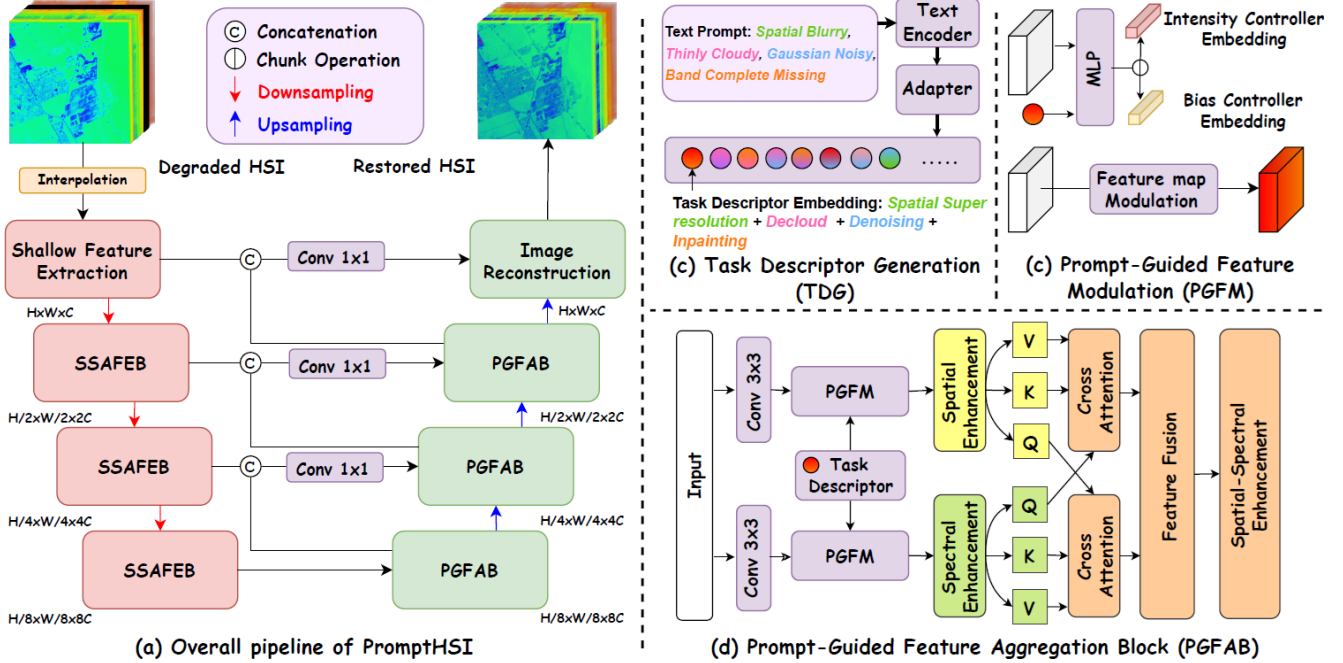


Figure 4. **The architecture of the proposed PromptHSI**, which is designed to tackle the composite degradations within a single universal model. First, we design a network based on U-net-like encoder-decoder architecture [45, 46] for capturing global spatial-spectral information, while combining Residual-Dense Group (RDG) and Fast-Residual-Dense Block (FRDB) presented in DRCT [17] and RTCS [16], respectively, in the proposed PGFAB for spatial-spectral enhancement. Afterwards, text-prompt-guidance and frequency-aware feature map modulation is proposed to jointly better capture the representation of composite degradation with controllability.

degraded HSI;  $\textcircled{2}$  A Prompt-Guided Feature Modulation (PGFM) that effectively bridging the domain gap between textual features and HSI features through frequency-domain modulation, while avoiding direct cross-domain feature alignment and information loss.

#### 4.1. Hyperspectral Image Restoration Pipeline

Our restoration pipeline consists of two key components: a SSAEFB for efficient feature extraction, and a PGFAB for controllable restoration with text-prompt guidance.

The encoder exploits the low-rank and sparse prior of HSIs through depth-wise separable convolution, effectively reducing computational complexity while preserving spectral characteristics. PGFAB then utilizes dual branches for spatial and spectral enhancement, with cross-attention mechanisms facilitating comprehensive feature integration.

**Spatial-spectral-aware encoder.** In conventional RGB restoration and other vision tasks, standard  $3 \times 3$  convolutions are widely considered to be sufficiently versatile and effective feature encoders. However, considering the low-rank characteristics of HSI, where substantial redundancy exists between different spectral bands, utilizing standard convolutions may reference unnecessary information from distant spectral bands, leading to suboptimal performance. Therefore, encoders based on lightweight convo-

lutions prove sufficiently effective while further reducing parameter size to meet practical application requirements.

Specifically, for the input HSI  $I_{\text{degraded}}$ , we first interpolate the spectrally discontinuous regions (caused by the stripe effect) to facilitate the learning process. Subsequently, we apply standard convolution layers to obtain shallow feature maps.

Afterwards, SSAFEs is based on a depth-wise separable convolution to extract features while inherently taking advantage of this low-rank prior, thereby reducing computational complexity without compromising performance [16].

**Prompt-guided feature aggregation block.** The features captured by SSAEFB are combined with the informative text-prompt guidance from PGFM (which will be discussed in the next subsection). Using effective guidance, the network is allowed to dynamically activate the corresponding weight for HSI restoration according to different types of degradation. To capture detailed information, PGFAB utilizes two distinct branches: one focuses on spatial dimension and the other on spectra. These branches are eventually integrated for feature aggregation.

**Spatial and spectral feature enhancement.** The output of PGFM is first improved by consecutive RDG [17] and FRDB [16] to improve fine-grained details. Then these features are interacted by cross-attention layer, which aims

to comprehensively integrate the spatial-spectral feature information from different branches across all dimensions. Specifically, it can be expressed as follows:

$$\{Q_\alpha, K_\alpha, V_\alpha\} = \mathcal{F}_{qkv}^\alpha(F_\alpha), \quad \{Q_\beta, K_\beta, V_\beta\} = \mathcal{F}_{qkv}^\beta(F_\beta), \quad (3)$$

where  $F_\alpha, F_\beta$  denote features from the spatial and spectral enhancement block. Subsequently, we exchange the queries  $Q$  of two branches for spatial-spectral interaction:

$$F_f^\beta = \text{softmax}\left(\frac{Q_\alpha K_\beta}{d_k}\right)V_\beta, \quad F_f^\alpha = \text{softmax}\left(\frac{Q_\beta K_\alpha}{d_k}\right)V_\alpha, \quad (4)$$

where  $d_k$  is the scaling factor. Subsequently, we concatenate the results obtained by the cross-attention through  $F_f^\gamma = \text{Concat}(F_f^\beta, F_f^\alpha)$  to obtain the integrated features.

$$\{Q_\gamma, K_\gamma, V_\gamma\} = \mathcal{F}_{qkv}^\gamma(F_f^\gamma), \quad \hat{F}_f^\gamma = \text{softmax}\left(\frac{Q_\gamma K_\gamma}{d_k}\right)V_\gamma, \quad (5)$$

Finally, we employ spectral-spatial self-attention for feature co-enhancement to improve representation capability.

Through a dual-branch architecture, we integrate text-prompt guidance effectively across both spatial and spectral dimensions. By incorporating plain-residual-in-residual [16, 17, 27] modules within the U-shape cascade decoder [8, 46], we enhance fine-grained image restoration while integrating global information, thereby effectively addressing various degradations for HSI restoration.

## 4.2. Prompt-Guided Feature Modulation

Directly using text features from VLMs for HSI restoration faces several critical challenges. Firstly, VLM features are trained on RGB-text pairs, lacking understanding of spectral characteristics and capturing complex spectral degradations. Secondly, their statistical distribution are mismatched because VLM features follow RGB image statistics, but HSI has essentially different data distributions, and direct adaptation requires complex domain translation.

Instead of directly bridging the HSI-text domain gap, our proposed PGFM addresses the domain gap by decomposing the problem into two easier sub-tasks. ❶ frequency-pattern matching with task descriptor and ❷ distribution adjustment by novel frequency-aware feature modulation mechanism. This strategy aim to selectively enhance spectral fidelity across frequency bands, thereby overcoming the limitations of text-guidance for avoiding direct cross-domain alignment between text features extracted from VLMs pre-trained on RGB-text domains and HSI.

**Task descriptor generation.** Given a text prompt  $T_{text}$  that provides the corresponding degradation description to guide the HSI restoration network to obtain the specified restoration result. In this study, we employ CLIP [40], which integrates vision and language information and performs effectively in text feature extraction. We freeze

the pre-trained CLIP to maintain great linguistic consistency and add additional MLP layer  $\Phi_t^{adpt.}$  as the feature adapter for pattern matching. With  $\{\cdot\}_e$  denoting the frozen weights, this process can be expressed as:

$$F_{text} = \Phi_t^{adpt.}(\{\mathcal{F}_{text}^{CLIP}\}_e(T_{text})), \quad (6)$$

where  $F_{text}$  denotes the task descriptors. With the task descriptors available, the next challenge is how to effectively incorporate this guidance into the HSI restoration process.

**Frequency-aware feature modulation.** Based on the frequency domain analysis, as illustrated in Section 3.2, we design our feature modulation mechanism to mimic how degradations affect different frequency components. Given an input feature map  $F_f$ , we first decompose it into frequency components:

$$F_f = F_f^l + F_f^h, \quad (7)$$

where  $F_f^l$  and  $F_f^h$  represent low and high frequency components, obtained through frequency-domain filtering.

Afterward, we design the MLP layer  $\Psi_m^i$  to extract this connection with the intensity and bias embeddings for feature modulation. Therefore, it can be obtained:

$$\lambda_m = \Psi_m^I(F_{text}), \quad \mu_m = \Psi_m^{II}(F_{text}), \quad (8)$$

where  $\Psi_m^I$  and  $\Psi_m^{II}$  are the chunk operations of  $\Psi_m$  to form the intensity and bias controller embeddings. To address the spectral consistency challenge in HSIs, our frequency-aware feature modulation adopts an affine transformation model tailored for spectral data, formulated as:

$$\hat{F}_f = (1 + \lambda_m^l) \odot F_f^l + (1 + \lambda_m^h) \odot F_f^h + \mu, \quad (9)$$

where Intensity controller  $\lambda \in [\lambda_m^l, \lambda_m^h]$  modulates the amplitude of high-frequency components to address noise, while Bias controller  $\mu$  shifts the low-frequency baseline to compensate for blurring and band-missing effects. This design ensures frequency-specific adjustments that RGB AiO frameworks lack.

To validate the efficacy of this mechanism, we performed ablation studies demonstrating improved spectral fidelity and PSNR consistency across spectral bands, underscoring the need for spectral domain modulation to manage complex HSI degradations effectively.

## 4.3. Loss Function

Given the wide range of spectra inherent in HSI, we utilize only the  $\ell_1$  loss for training. However, this strategy may not adequately capture the variability across different bands. Consequently, the  $\ell_1$  loss might inadvertently focus on minimizing bands with larger values, affecting the spectral integrity of specific bands.

**Spectral angle mapper loss.** SAM metric is also critical for material identification and less sensitive to intensity

Table 1. **Overall performance evaluation for composite degradation and complexity comparison.** To simulate composite degradations, we maintain a fixed  $p$  of 0.5 for triggering individual degradation types, as demonstrated in Figure 2, for all experiments. Note that **Cr.** means **Controllable** or **Not**. As for the complexity parts, M and G indicate  $10^6$  and  $10^9$ , respectively. The best, second-best and third-best results are highlighted in **bold-red**, **bold-blue**, and **bold-green**, respectively.

Type	Methods	Venue & Year	Task	Domain	Cr.	PSNR $\uparrow$	SAM $\downarrow$	RMSE $\downarrow$	ERGAS $\downarrow$	#Params $\downarrow$	FLOPs $\downarrow$
Input	-	-	-	-	-	-	-	-	-	-	-
One-to-One	HSIDwRD [49]	ICCV 2021	Denoising	HSI	×	20.6270	12.7891	0.0364	97.3601	23.62M	5054.16G
	SERT [25]	CVPR 2023	Denoising	HSI	×	16.1657	15.9853	0.0348	29.2053	2.74M	176.06 G
	SRDNet [33]	TGRS 2024	Super-Res.	HSI	×	19.0520	11.9590	0.0320	<b>16.5861</b>	1.86M	3771.80G
	SNLSR [19]	TIP 2024	Super-Res.	HSI	×	17.8785	20.4389	0.0445	19.1267	1.75M	14.20G
	SGNet [35]	ISPRS 2022	Decloud	HSI	×	18.0694	12.9476	0.0359	17.9773	0.54M	57.39G
	AACNet [48]	TGRS 2023	Decloud	HSI	×	17.6279	14.5962	0.0324	26.2115	2.76M	171.23G
	SST [24]	AAAI 2023	Inpainting	HSI	×	18.9792	10.9860	<b>0.0244</b>	26.9934	4.30M	281.72G
	HSDT [22]	ICCV 2023	Inpainting	HSI	×	18.0665	11.3451	0.0372	68.4451	0.51M	67.55G
All-in-One for specific	AirNet [23]	CVPR 2022	-	RGB	×	<b>23.6647</b>	<b>7.5970</b>	<b>0.0233</b>	<b>16.4194</b>	6.07M	245.86G
	PromptIR [39]	NeurIPS 2023	-	RGB	×	17.2667	<b>9.6437</b>	0.0405	29.2768	33.18M	132.07G
	HAIR [5]	arXiv 2024	-	RGB	×	<b>20.5779</b>	14.4329	0.0275	24.4211	7.86M	42.51G
	InstructIR [10]	ECCV 2024	-	RGB	✓	20.3106	14.5727	0.0306	27.5454	16.02M	17.28G
All-in-One for composite	OneRestore [13]	ECCV 2024	-	RGB	✓	17.3321	15.0320	0.0271	52.1162	5.85M	12.05G
	<b>PromptHSI (Ours)</b>	-	-	HSI	✓	<b>26.4432</b>	<b>6.0601</b>	<b>0.0185</b>	<b>8.3566</b>	26.14M	135.83G

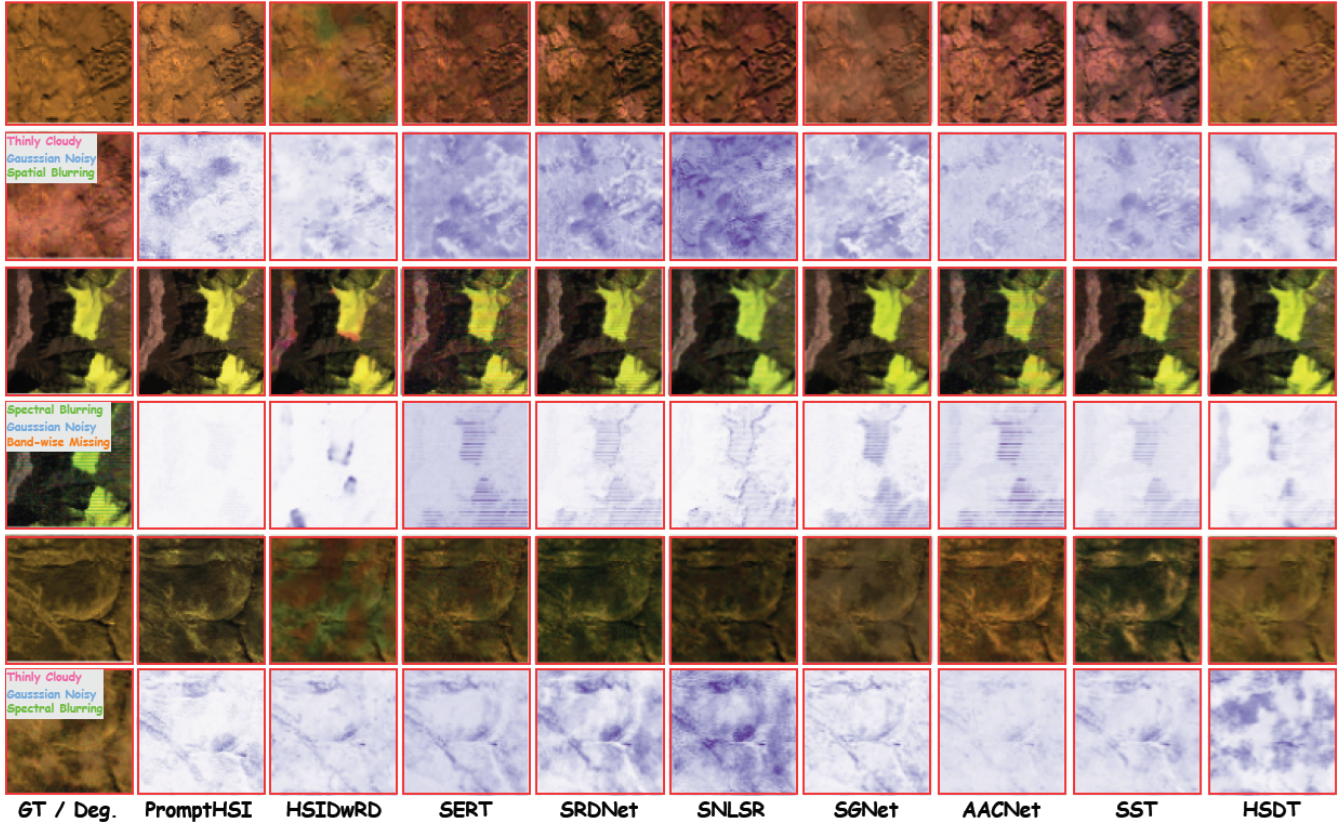


Figure 5. **Visualization results for HSI restoration methods.** *top*: the reconstructed HSI, *bottom*: the residual image derived from Ground-truth and reconstructed result. Most of state-of-the-arts HSI restoration methods fail to deal with composite degradations.

variations. The  $\ell_{\text{SAM}}$  loss prioritizes angular discrepancies over magnitudes, offering a reliable metric to evaluate the

spectral fidelity of the reconstructed HSI.

$$\ell_{\text{SAM}} = \frac{1}{N} \sum_{n=1}^N \cos^{-1} \left( \frac{I_n^T I_n^* + \epsilon}{\|I_n\|_2 \cdot \|I_n^*\|_2 + \epsilon} \right), \quad (10)$$

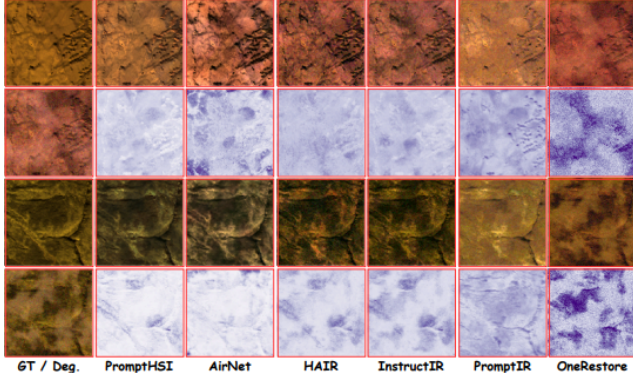


Figure 6. **Comparison for AiO RGB image restoration methods.** For the text-prompt-based methods [10, 13] and our PromptHSI, we employ the standard text-prompts presented in this study for training network and inference for related experiments.

where  $I_n$  and  $I_n^*$  represent the  $n$ -th spectral vector of the ground-truth and the reconstructed HSI, respectively. The term  $\epsilon$  is included to avoid divergence.

**Stationary wavelet transform loss.** Wavelet sub-band alignment is able to manage various aspects of information encoded in HSIs. On the other words, it facilitates more detailed supervision in the frequency-domain.

$$\ell_{\text{SWT}} = \sum_j \lambda_j \|\text{SWT}(I)_j - \text{SWT}(I^*)_j\|_1, \quad (11)$$

where  $\lambda_j$  represents the count of sub-bands decomposed via stationary wavelet transformation.

**Band-wise MSE loss.** The band-wise disparity helps stabilize the network optimization process and is advantageous to achieve convergence, balancing restoration quality across all spectra. The Band-wise MSE loss can be simply defined as follows:

$$\ell_{\text{BMSE}} = \frac{1}{N} \sum_{n=1}^N \|I_n - I_n^*\|_2, \quad (12)$$

**Total loss.** Ultimately, the total loss function for training the proposed PromptHSI  $\ell_{\text{total}}$  can be expressed as:

$$\ell_{\text{total}} = \lambda_1 \ell_1 + \lambda_2 \ell_{\text{SAM}} + \lambda_3 \ell_{\text{SWT}} + \lambda_4 \ell_{\text{BMSE}}, \quad (13)$$

where  $\lambda_{1,2,3,4}$  serve as the weighting coefficients to equilibrate  $\ell_1$ ,  $\ell_{\text{SAM}}$ ,  $\ell_{\text{SWT}}$ , and  $\ell_{\text{BMSE}}$ , set at 1, 0.1, 0.01, 0.01 throughout all experiments, respectively.

## 5. Experimental Results

**Experiment Setup.** This study employed the AVIRIS dataset provided by Lin *et al.* [18, 30], an extensive HSI dataset, with numerous bands spanning diverse geographical areas for experiments. It includes 2,078 HSIs, which

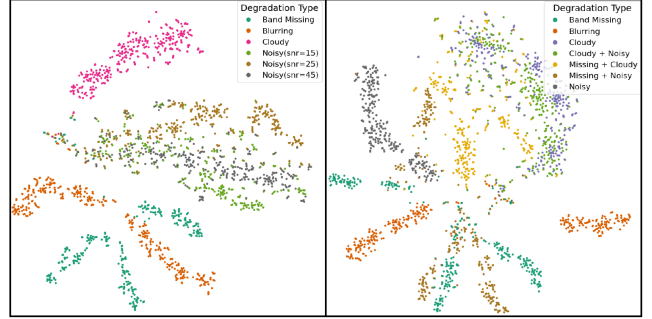


Figure 7. **Comparison of t-SNE visualization results** for the degradation embeddings of the proposed PromptHSI trained on single degradation. (a) for multiple degradation, (b) for composite degradation. The proposed PromptHSI have demonstrated its discriminative capability in identifying different degradation even unseen degradation and its combination during testing-time.

were randomly divided into training, validation, and testing sets. The training set consisted of 1,678 images and both the validation and testing sets contained 200 images each. As illustrated in **Supplementary**, all clean HSI was pre-processed to synthesize the composite degraded HSIs and corresponding text descriptions.

### 5.1. Quantitative Results and Analysis

To evaluate the performance of PromptHSI, we compared it with eight other supervised HSI restoration methods for specific degradation, including HSIDwRD [49], SERT [25], SRDNet [33], SNLSR [19], SGNet [35], AACNet [48], SST [24], and HSDT [22] in the synthesized AVIRIS dataset with composite degradations. Because there is no AiO HSI restoration method, we compare four AiO RGB image restoration methods in the experiments: AirNet [23], PromptIR [39], HAIR [5], InstructIR [10], and OneRestore [13]. The model performance was measured using the four metrics, including PSNR, SAM, RMSE, and ERGAS. Table 1 presents the quantitative results.

**Ours vs. Task-specific HSI restoration methods.** All peer-methods fail to effectively recover the degraded HSIs due to their ability to learn different or unseen degradations. In contrast, PromptHSI can restore better even without text-prompt, as shown in Table 4, which exhibits the capability of our unified restoration network design.

**Ours vs. All-in-One RGB restoration methods.** Unlike AiO RGB image restoration methods that rely on uniform feature modulation, our PromptHSI framework’s frequency-aware modulation dynamically tailors restoration to each spectral band, thereby achieving cross-band consistency crucial for HSI applications.

In general, our PromptHSI exceeds other AiO methods. Firstly, most of existing methods struggle to handle composite degradations. As discussed previously, both data and

Table 2. Ablation of integration strategy.

Strategy	PSNR / SAM / RMSE / EGRAS
Intensity-only	<b>26.0070 / 6.3636 / 0.0187 / 9.7608</b>
Bias-only	25.6384 / 6.3963 / 0.0190 / 12.4992
Weighted-sum	25.7284 / 6.3561 / 0.0188 / 14.3605
<b>Intensity &amp; Bias</b>	<b>26.4432 / 6.0601 / 0.0185 / 8.3566</b>

Table 3. Effect of prompting method.

Prompt type	Cr.	PSNR / SAM / RMSE / EGRAS
RGB to VLM	×	24.1273 / 7.6236 / 0.0257 / 14.5208
Hybrid to VLM	✓	<b>25.2385 / 6.8974 / 0.0191 / 11.4359</b>
PGB & PIM [39]	×	23.0567 / 9.4862 / 0.0287 / 24.5575
<b>Text to VLM</b>	✓	<b>26.4432 / 6.0601 / 0.0185 / 8.3566</b>

Table 4. Ablation of network component.

	Without	PSNR / SAM / RMSE / EGRAS
<b>Full model</b>		<b>26.4432 / 6.0601 / 0.0185 / 8.3566</b>
PGFM		25.4905 / 6.6348 / 0.0205 / 13.2072
adapter		25.8686 / 6.3561 / 0.0188 / 14.3605
enhancement		23.7511 / 7.9918 / 0.0262 / 16.0007

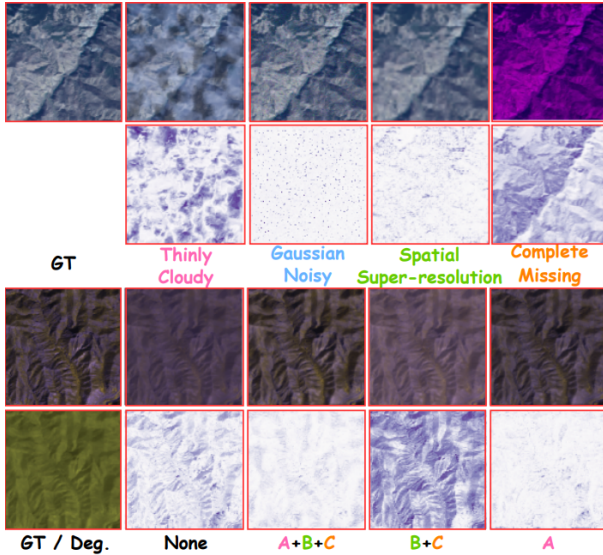


Figure 8. **Visualization results for the controllability.** *Top*, for single-specific degradation, the plots in the first row represent the degraded HSI, while the second row shows residual maps, obtained from the reconstructed HSI, with or without the guidance provided by the text-prompt. *Bottom*, in the case of composite degradation, the top row of plots depicts the recovered HSI, while the residual maps are obtained from the reconstructed HSI using the specified text-prompt guidance with the ground-truth.

features extracted by pre-trained CLIP [40] exhibit domain gaps with HSI. Therefore, these models are not effective in transferring to AiO HSI restoration.

Specifically, OneRestore [13] incorporated task description features into its encoder block, which hindered its capacity to accurately capture the spatial-spectral correlation in HSI because of the domain gap with HSI features, resulting in decoding failures. Moreover, it lacks considerations for tasks requiring high-frequency detail reconstruction, potentially limiting its effectiveness in the spatial or spectral super-resolution task.

## 5.2. Ablation Studies and Analysis

The aforementioned experimental results demonstrate the effectiveness of our proposed PromptHSI framework under composite degradations. We further conduct ablation studies to investigate the impact of different components and strategies.

**Integration strategy of feature-map modulation.** As shown in Table 2, our proposed frequency-aware feature

modulation demonstrates superior effectiveness compared to the weighted-sum manner, where we implemented an MLP layer for dynamic weighted averaging of inputs and outputs. The intensity-only configuration outperforms the bias-only, with a notably larger advantage in the ERGAS metric, suggesting that this integration strategy effectively guides network restoration across most scenarios.

**Visual-prompt or text-prompt.** The type of prompting is crucial, as it determines its ability to recognize various degradations and effectively guide and control model behavior. In the first configuration, we select RGB bands from HSIs as visual prompts, encoding them through CLIP [40] and using the proposed PGFM to guide the model. Secondly, we encode both RGB bands and textual prompts to generate hybrid task descriptors for guidance. In the final configuration, we remove PGFM and use the PIM and PGM block proposed in PromptIR [39] for the generation of visual prompts and interaction of features.

The experimental results are presented in Table 3. Due to multiple or composite degradations in the spatial-domain leading to serious information loss, it became difficult to obtain compact task descriptors or valid visual prompts, ultimately resulting in diminished prompt effectiveness and compromised restoration. The use of textual features helps to circumvent these issues and achieves robust prompting guidance through semantic information.

**Ablation of network component.** To understand the impact of the network components, we performed ablation studies by removing PGFM, adapter and spatial spectral enhancement from the network, with results shown in Table 4. Even without textual features, our proposed PromptHSI outperforms other peer methods in handling composite degradation, demonstrating the effectiveness and universality of our network architecture. The adapter proves crucial in bridging the domain gap between the VLM and HSI features via pattern matching, leading to improved global reconstruction performance, particularly evident in the ERGAS metric. Lastly, we can observe that there is a drop with or without spatial-spectral enhancement, which represents that feature enhancement is essential for details recovery within cascade decoder.

These results demonstrate PromptHSI’s superior capability in maintaining spectral fidelity across multiple degradation types, highlighting the necessity of frequency-aware modulation, particularly when compared to AiO RGB methods that exhibit substantial performance degradation in the HSI domain. In summary, PromptHSI offers a universal

and controllable solution for addressing composite degradation in real-world applications.

## 6. Conclusion

In this paper, we present PromptHSI, the first universal framework for hyperspectral image restoration that effectively addresses composite degradations, which conventional HSI restoration methods have failed to handle. Unlike existing All-in-One RGB image restoration approaches that struggle with domain gaps between RGB and HSI features and structures, our method is specifically designed to address HSI-specific attributes and commonly encountered degradation patterns. Then, our method is controllable through text-prompt guidance, based on a novel frequency-aware modulation strategy that effectively bridges the gap between text and HSI through frequency pattern matching and distribution adjustment in the frequency-domain. Our approach demonstrates superior performance across various types of degradation and their combinations, significantly outperforming existing methods.

## References

- [1] Jose M. Bioucas-Dias, Antonio Plaza, Gustavo Camps-Valls, Paul Scheunders, Nasser Nasrabadi, and Jocelyn Chanussot. Hyperspectral remote sensing data analysis and future challenges. *IEEE Geoscience and Remote Sensing Magazine*, 1(2):6–36, 2013. 1
- [2] Yuanhao Cai, Jing Lin, Xiaowan Hu, Haoqian Wang, Xin Yuan, Yulun Zhang, Radu Timofte, and Luc Van Gool. Mask-guided spectral-wise transformer for efficient hyperspectral image reconstruction. In *CVPR*, 2022. 2
- [3] Yuanhao Cai, Jing Lin, Zudi Lin, Haoqian Wang, Yulun Zhang, Hanspeter Pfister, Radu Timofte, and Luc Van Gool. Mst++: Multi-stage spectral-wise transformer for efficient spectral reconstruction. In *CVPRW*, 2022. 2
- [4] Yuanhao Cai, Jing Lin, Haoqian Wang, Xin Yuan, Henghui Ding, Yulun Zhang, Radu Timofte, and Luc Van Gool. Degradation-aware unfolding half-shuffle transformer for spectral compressive imaging. In *NeurIPS*, 2022. 1
- [5] Jin Cao, Yi Cao, Li Pang, Deyu Meng, and Xiangyong Cao. Hair: Hypernetworks-based all-in-one image restoration, 2024. 1, 2, 3, 6, 7
- [6] Daniele Cerra, Rupert Müller, and Peter Reinartz. Unmixing-based denoising for destriping and inpainting of hyperspectral images. In *2014 IEEE Geoscience and Remote Sensing Symposium*, pages 4620–4623, 2014. 2
- [7] Wei-Ting Chen, Zhi-Kai Huang, Cheng-Che Tsai, Hao-Hsiang Yang, Jian-Jiun Ding, and Sy-Yen Kuo. Learning multiple adverse weather removal via two-stage knowledge learning and multi-contrastive regularization: Toward a unified model. In *2022 IEEE/CVF Conference on Computer Vision and Pattern Recognition (CVPR)*, pages 17632–17641, 2022. 2
- [8] Xiangyu Chen, Zheyuan Li, Yuandong Pu, Yihao Liu, Jiantao Zhou, Yu Qiao, and Chao Dong. A comparative study of image restoration networks for general backbone network design. In *European Conference on Computer Vision (ECCV)*, 2024. 3, 5
- [9] Zheng Chen, Zongwei Wu, Eduard-Sebastian Zamfir, Kai Zhang, Yulun Zhang, Radu Timofte, Xiaokang Yang, et al. Ntire 2024 challenge on image super-resolution (x4): Methods and results. In *Computer Vision and Pattern Recognition Workshops (CVPRW)*, 2024. 3
- [10] Marcos V Conde, Gregor Geigle, and Radu Timofte. Instructir: High-quality image restoration following human instructions. In *Proceedings of the European Conference on Computer Vision (ECCV)*, 2024. 1, 2, 3, 6, 7
- [11] Keivan Faghieh Niresi and Chong-Yung Chi. Robust hyperspectral inpainting via low-rank regularized untrained convolutional neural network. *IEEE Geoscience and Remote Sensing Letters*, 20:1–5, 2023. 1, 2
- [12] Qingnan Fan, Dongdong Chen, Lu Yuan, Gang Hua, Nenghai Yu, and Baoquan Chen. A general decoupled learning framework for parameterized image operators. *IEEE Transactions on Pattern Analysis and Machine Intelligence*, 43(1): 33–47, 2021. 2
- [13] Yu Guo, Yuan Gao, Yuxu Lu, Ryan Wen Liu, and Shengfeng He. Onerestore: A universal restoration framework for composite degradation. In *European Conference on Computer Vision (ECCV)*, 2024. 1, 2, 3, 6, 7, 8
- [14] Jiang He, Qiangqiang Yuan, Jie Li, Yi Xiao, Denghong Liu, Huanfeng Shen, and Liangpei Zhang. Spectral super-resolution meets deep learning: Achievements and challenges. *Information Fusion*, 97:101812, 2023. 2
- [15] Wei He, Quanming Yao, Chao Li, Naoto Yokoya, and Qibin Zhao. Non-local meets global: An integrated paradigm for hyperspectral denoising. In *2019 IEEE/CVF Conference on Computer Vision and Pattern Recognition (CVPR)*, pages 6861–6870, 2019. 2
- [16] Chih-Chung Hsu, Chih-Yu Jian, Eng-Shen Tu, Chia-Ming Lee, and Guan-Lin Chen. Real-time compressed sensing for joint hyperspectral image transmission and restoration for cubesat. *IEEE Transactions on Geoscience and Remote Sensing*, 2024. 4, 5
- [17] Chih-Chung Hsu, Chia-Ming Lee, and Yi-Shiuan Chou. Drct: Saving image super-resolution away from information bottleneck. In *Proceedings of the IEEE/CVF Conference on Computer Vision and Pattern Recognition (CVPR) Workshops*, pages 6133–6142, 2024. 3, 4, 5
- [18] Chih-Chung Hsu, Chih-Chien Ni, Chia-Ming Lee, and Li-Wei Kang. Csakd: Knowledge distillation with cross self-attention for hyperspectral and multispectral image fusion, 2024. 2, 7
- [19] Qian Hu, Xinya Wang, Junjun Jiang, Xiao-Ping Zhang, and Jiayi Ma. Exploring the spectral prior for hyperspectral image super-resolution. *IEEE Transactions on Image Processing*, 33:5260–5272, 2024. 1, 3, 6, 7
- [20] Junjun Jiang, He Sun, Xianming Liu, and Jiayi Ma. Learning spatial-spectral prior for super-resolution of hyperspectral imagery. *IEEE Transactions on Computational Imaging*, 6:1082–1096, 2020. 2

- [21] Yo-Yu Lai, Chia-Hsiang Lin, and Zi-Chao Leng. Hyperrestormer: A general hyperspectral image restoration transformer for remote sensing imaging, 2023. 3
- [22] Zeqiang Lai, Yan Chenggang, and Ying Fu. Hybrid spectral denoising transformer with guided attention. In *Proceedings of the IEEE International Conference on Computer Vision*, 2023. 1, 6, 7
- [23] Boyun Li, Xiao Liu, Peng Hu, Zhongqin Wu, Jiancheng Lv, and Xi Peng. All-In-One Image Restoration for Unknown Corruption. In *IEEE Conference on Computer Vision and Pattern Recognition*, New Orleans, LA, 2022. 2, 6, 7
- [24] Miaoyu Li, Ying Fu, and Yulun Zhang. Spatial-spectral transformer for hyperspectral image denoising. In *AAAI*, 2023. 1, 2, 6, 7
- [25] Miaoyu Li, Ji Liu, Ying Fu, Yulun Zhang, and Dejing Dou. Spectral enhanced rectangle transformer for hyperspectral image denoising. In *CVPR*, 2023. 1, 6, 7
- [26] Yong Li, Lei Zhang, Chen Dingli, Wei Wei, and Yanning Zhang. Single hyperspectral image super-resolution with grouped deep recursive residual network. In *2018 IEEE Fourth International Conference on Multimedia Big Data (BigMM)*, pages 1–4, 2018. 2
- [27] Jingyun Liang, Jiezhong Cao, Guolei Sun, Kai Zhang, Luc Van Gool, and Radu Timofte. Swinir: Image restoration using swin transformer. *arXiv preprint arXiv:2108.10257*, 2021. 3, 5
- [28] Chia-Hsiang Lin, Tzu-Hsuan Lin, Ting-Hsuan Lin, and Tang-Huang Lin. Fast reconstruction of hyperspectral image from its rgb counterpart using admm-adam theory. In *2022 12th Workshop on Hyperspectral Imaging and Signal Processing: Evolution in Remote Sensing (WHISPERS)*, pages 1–5, 2022. 1
- [29] Chia-Hsiang Lin, Yen-Cheng Lin, and Po-Wei Tang. Admm-adam: A new inverse imaging framework blending the advantages of convex optimization and deep learning. *IEEE Transactions on Geoscience and Remote Sensing*, 60:1–16, 2022. 1, 2
- [30] Chia-Hsiang Lin, Chih-Chung Hsu, Si-Sheng Young, Cheng-Ying Hsieh, and Shen-Chieh Tai. Qrcode: Quasi-residual convex deep network for fusing misaligned hyperspectral and multispectral images. *IEEE Transactions on Geoscience and Remote Sensing*, 62:1–15, 2024. 7
- [31] Jingbo Lin, Zhilu Zhang, Yuxiang Wei, Dongwei Ren, Dongsheng Jiang, Qi Tian, and Wangmeng Zuo. Improving image restoration through removing degradations in textual representations. In *2024 IEEE/CVF Conference on Computer Vision and Pattern Recognition (CVPR)*, pages 2866–2878, 2024. 1
- [32] Yu-Fan Lin, Ching-Heng Cheng, Bo-Cheng Qiu, Cheng-Jun Kang, Chia-Ming Lee, and Chih-Chung Hsu. Self-supervised fusarium head blight detection with hyperspectral image and feature mining, 2024. 1
- [33] Tingting Liu, Yuan Liu, Chuncheng Zhang, Liyin Yuan, Xiubao Sui, and Qian Chen. Hyperspectral image super-resolution via dual-domain network based on hybrid convolution. *IEEE Transactions on Geoscience and Remote Sensing*, 62:1–18, 2024. 1, 3, 6, 7
- [34] Qing Ma, Junjun Jiang, Xianming Liu, and Jiayi Ma. Deep unfolding network for spatospectral image super-resolution. *IEEE Transactions on Computational Imaging*, 8:28–40, 2022. 1
- [35] Xiaofeng Ma, Qunming Wang, and Xiaohua Tong. A spectral grouping-based deep learning model for haze removal of hyperspectral images. *ISPRS Journal of Photogrammetry and Remote Sensing*, 188:177–189, 2022. 1, 6, 7
- [36] Matteo Maggioni, Vladimir Katkovnik, Karen Egiazarian, and Alessandro Foi. Nonlocal transform-domain filter for volumetric data denoising and reconstruction. *IEEE Transactions on Image Processing*, 22(1):119–133, 2013. 2
- [37] Sina Nakhostin, Harold Clenet, Thomas Corpetti, and Nicolas Courty. Joint anomaly detection and spectral unmixing for planetary hyperspectral images. *IEEE Transactions on Geoscience and Remote Sensing*, 54(12):6879–6894, 2016. 1
- [38] Jiangjun Peng, Hailin Wang, Xiangyong Cao, Xinling Liu, Xiangyu Rui, and Deyu Meng. Fast noise removal in hyperspectral images via representative coefficient total variation. *IEEE Transactions on Geoscience and Remote Sensing*, 60:1–17, 2022. 2
- [39] Vaishnav Potlapalli, Syed Waqas Zamir, Salman Khan, and Fahad Khan. Promptir: Prompting for all-in-one image restoration. In *Thirty-seventh Conference on Neural Information Processing Systems*, 2023. 1, 2, 3, 6, 7, 8
- [40] Alec Radford, Jong Wook Kim, Chris Hallacy, Aditya Ramesh, Gabriel Goh, Sandhini Agarwal, Girish Sastry, Amanda Askell, Pamela Mishkin, Jack Clark, et al. Learning transferable visual models from natural language supervision. *arXiv preprint arXiv:2103.00020*, 2021. 2, 5, 8
- [41] Bin Ren, Yawei Li, Nancy Mehta, and Radu et al. Timofte. The ninth ntire 2024 efficient super-resolution challenge report. In *Proceedings of the IEEE/CVF Conference on Computer Vision and Pattern Recognition (CVPR) Workshops*, pages 6595–6631, 2024. 3
- [42] Feng Shi, Jian Cheng, Li Wang, Pew-Thian Yap, and Dinggang Shen. Lrtv: Mr image super-resolution with low-rank and total variation regularizations. *IEEE Transactions on Medical Imaging*, 34(12):2459–2466, 2015. 1, 2
- [43] Oleksii Sidorov and Jon Yngve Hardeberg. Deep hyperspectral prior: Single-image denoising, inpainting, super-resolution. In *Proceedings of the IEEE/CVF International Conference on Computer Vision (ICCV) Workshops*, 2019. 1, 2
- [44] Gregg Vane, Robert Green, Thomas Chrien, Harry Enmark, Earl Hansen, and Wallace Porter. The airborne visible/infrared imaging spectrometer (aviris). *Remote Sensing of Environment*, 44(2-3):127–143, 1993. 1
- [45] Zhendong Wang, Xiaodong Cun, Jianmin Bao, Wengang Zhou, Jianzhuang Liu, and Houqiang Li. Uformer: A general u-shaped transformer for image restoration. In *Proceedings of the IEEE/CVF Conference on Computer Vision and Pattern Recognition (CVPR)*, pages 17683–17693, 2022. 3, 4
- [46] Syed Waqas Zamir, Aditya Arora, Salman Khan, Munawar Hayat, Fahad Shahbaz Khan, and Ming-Hsuan Yang. Restormer: Efficient transformer for high-resolution image restoration. In *CVPR*, 2022. 3, 4, 5

- [47] Zhijian Wu, Jun Li, Chang Xu, Dingjiang Huang, and Steven C. H. Hoi. Run: Rethinking the unet architecture for efficient image restoration. *IEEE Transactions on Multimedia*, 26: 10381–10394, 2024. [3](#)
- [48] Meng Xu, Yanxin Peng, Ying Zhang, Xiuping Jia, and Sen Jia. Aacnet: Asymmetric attention convolution network for hyperspectral image dehazing. *IEEE Transactions on Geoscience and Remote Sensing*, 61:1–14, 2023. [1](#), [6](#), [7](#)
- [49] Tao Zhang, Ying Fu, and Cheng Li. Hyperspectral image denoising with realistic data. In *Proceedings of the IEEE/CVF International Conference on Computer Vision (ICCV)*, pages 2248–2257, 2021. [1](#), [6](#), [7](#)
- [50] Yulun Zhang, Kunpeng Li, Kai Li, Lichen Wang, Bineng Zhong, and Yun Fu. Image super-resolution using very deep residual channel attention networks. In *ECCV*, 2018. [3](#)
- [51] Yulun Zhang, Kai Zhang, Zheng Chen, Yawei Li, and Radu et al. Timofte. Ntire 2023 challenge on image super-resolution (x4): Methods and results. In *Proceedings of the IEEE/CVF Conference on Computer Vision and Pattern Recognition (CVPR) Workshops*, pages 1865–1884, 2023. [3](#)
- [52] Lina Zhuang and José M. Bioucas-Dias. Fast hyperspectral image denoising and inpainting based on low-rank and sparse representations. *IEEE Journal of Selected Topics in Applied Earth Observations and Remote Sensing*, 11(3): 730–742, 2018. [1](#), [2](#)